

TECHNICAL MEMORANDUM

X-539

DAMPING IN PITCH AND STATIC STABILITY OF
BLUNT CONE-CYLINDER-FLARE MODELS AND
MANNED REENTRY CAPSULE MODELS FOR
VARIOUS ANGLES OF ATTACK AT

A MACH NUMBER OF 2.91

By Herman S. Fletcher

Langley Research Center
Langley Field, Va.

NATIONAL AERONAUTICS AND SPACE ADMINISTRATION
WASHINGTON

July 1961

~~CONFIDENTIAL~~

REF ID: A65571

NATIONAL AERONAUTICS AND SPACE ADMINISTRATION

TECHNICAL MEMORANDUM X-539

DAMPING IN PITCH AND STATIC STABILITY OF

BLUNT CONE-CYLINDER-FLARE MODELS AND

MANNED REENTRY CAPSULE MODELS FOR

VARIOUS ANGLES OF ATTACK AT

A MACH NUMBER OF 2.91*

By Herman S. Fletcher

SUMMARY

An experimental investigation has been made at a Mach number of 2.91 to determine the damping-in-pitch and static-stability parameters of six blunt cone-cylinder-flare (supersonic-impact) models, a blunt cylinder flare (subsonic-impact) model, three manned reentry capsule models, and a slightly blunted cone model. The tests were made at angles of attack from 0° to 14.10° and at initial amplitudes from 0.82° to 3.23° by using a single-degree-of-freedom free-oscillation technique. The Reynolds number, based on maximum model diameter, varied from 0.44×10^6 to 1.76×10^6 . Theoretical values of the damping-in-pitch and static-stability parameters obtained by using Newtonian impact theory and combined first- and second-order cone theory are presented for comparison with the test data.

The results showed that all the models had favorable damping-in-pitch and static-stability parameters and that a decrease in oscillation amplitude decreased the damping at the lower angles of attack. The variation of the damping with increase in angle of attack showed no consistent trends, but decreased and then increased with angle of attack for some models but not for others. This erratic behavior tended to become smaller or disappear at the higher Reynolds number. The static-stability parameter of the models generally increased with increase in angle of attack; the effects of oscillation amplitude on this parameter were negligible.

INTRODUCTION

The Langley Research Center has initiated a research program to determine the static and dynamic stability characteristics of a variety of reentry shapes which include blunt cone-cylinder-flare (supersonic-impact) models, blunt cylinder-flare (subsonic-impact) models, and high-drag low-lift manned reentry capsule models. This program provides for tests in several Langley facilities in the subsonic, supersonic, and hypersonic speed regimes and through a large Reynolds number range.

Some portions of this program already have been completed and the results have been published. Static longitudinal stability characteristics for the supersonic-impact ballistic missiles are presented in references 1 and 2 for Mach numbers between 1.47 and 3.05. Dynamic stability data obtained from free-oscillation tests about an angle of attack of 0° are presented for the ballistic missiles, high-drag reentry capsules, and other short blunt-nosed configurations in reference 3 for Mach numbers of 1.93 to 3.05 and in reference 4 for a Mach number of 6.83. No damping data are available, however, for these configurations at angles of attack other than 0° or at oscillation amplitudes other than approximately 3° . Some dynamic- and static-stability data at various angles of attack are available for blunt-nosed cylinder-flare bodies in reference 5 and for bluff bodies of revolution in reference 6.

As part of the continuing program to provide stability data for this wide range of configurations, the present investigation was initiated to provide data on the damping and static stability at various angles of attack up to approximately 15° for configurations representative of these ballistic missiles and manned reentry capsules. The models were tested in the Langley 9-inch supersonic tunnel at a Mach number of 2.91 by using a free-to-damp oscillation technique. Values for the dynamic- and static-stability derivatives calculated from the methods given in reference 7 (Newtonian impact theory) and from the combined first- and second-order cone theory given in reference 8 also are presented.

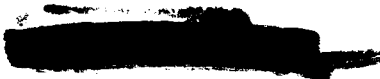
SYMBOLS

A	maximum cross-sectional area of model, sq ft
d	maximum diameter of model, ft
I	moment of inertia in pitch, slug-ft ²
K	spring constant, ft-lb/radian

- k reduced-frequency parameter, $\omega d/2V$
- M Mach number
- M_Y pitching moment about center of gravity, ft-lb
- P period of oscillation, sec
- q pitching velocity, radians/sec
- q_∞ free-stream dynamic pressure, $\frac{\rho V^2}{2}$, lb/sq ft
- $\dot{q} = \frac{\partial q}{\partial t}$, radians/sec²
- R Reynolds number
- t time, sec
- $t_{1/2}$ time to damp to one-half amplitude, sec
- V velocity, ft/sec
- α angle of attack, radians
- $\dot{\alpha} = \frac{\partial \alpha}{\partial t}$, radians/sec
- α_m true angle of attack about which model oscillates, deg
- α_s sting angle, deg
- θ_o maximum amplitude about α_m , deg
- ρ mass density, slugs/cu ft
- ω circular frequency, radians/sec

$$C_m = \frac{M_Y}{q_\infty A d}$$

$$C_{m\alpha} = \frac{\partial C_m}{\partial \alpha}$$



0317125530

03

$$C_{m\dot{\alpha}} = \frac{\partial C_m}{\partial \left(\frac{\dot{\alpha} d}{2V} \right)}$$

$$C_{mq} = \frac{\partial C_m}{\partial \left(\frac{q d}{2V} \right)}$$

$$C_{m\dot{q}} = \frac{\partial C_m}{\partial \left(\frac{\dot{q} d^2}{4V^2} \right)}$$

$C_{m\alpha} - k^2 C_{m\dot{q}}$ static-stability parameter, per radian

$C_{mq} + C_{m\dot{\alpha}}$ dynamic-stability (or damping-in-pitch) parameter, per radian

Subscript:

ω signifies a derivative measured from an oscillation test

MODELS

Side-view drawings of the models (bodies of revolution) are shown in figure 1. A photograph of the models is shown as figure 2. Models 1, 2, 3, and 4 had identical nose shapes, which were truncated cones having a semiapex angle of 20° , and differed only in afterbody shape. For model 1 the afterbody flare angle was a constant 3.87° . Model 2 had a cylindrical afterbody with a 5.35° tail flare, and model 3 had a cylindrical afterbody with a 10° tail flare. It should be pointed out here that in order to increase the flare angle while maintaining the same base diameter the location of the cylinder flare juncture, of necessity, moved rearward on the bodies of these models. Model 4 had six 86.23° sweptback fins which were evenly spaced around the cylindrical afterbody and attached to the model for its entire cylindrical length. Models 5 and 6 were identical to models 1 and 3, respectively, except for the nose shape which had been lengthened in order to decrease the severity of the bluntness. Model 7 was a blunt-faced cylinder with a 10° flared tail, and model 8 was a slightly blunt cone having a semiapex angle of 7.5° . Models 9, 10, and 11 were blunt-faced configurations representative of manned reentry capsules.

DECLASSIFIED

5

Each model was machined from aluminum and mass-balanced so that the center of gravity coincided with the pivot axis of the crossed-flexure strain gage. The static-stability and damping-in-pitch measurements presented herein are referred to the center-of-gravity position shown in figure 1. Mass characteristics for the models are given in table I.

INSTRUMENTATION

The models were oscillated on a crossed-flexure strain gage (fig. 3), the output signals of which were proportional to the model angular displacement in pitch. A flexure strain gage was chosen for these tests because it allowed the internal friction or wind-off damping to be determined readily and consistently and thus permitted good repeatability of the data. The strain-gage signal was amplified and fed into the recorder where a spotlight galvanometer converted the electrical signal into an optical signal. The optical signal, in turn, was recorded on photographic paper.

TUNNEL AND TESTS

The single-degree-of-freedom free-oscillation tests of this investigation were made in the Langley 9-inch supersonic tunnel (fig. 4). This tunnel is a continuous-operation complete-return type in which Reynolds number, stagnation temperature, and Mach number can be varied and controlled. The variation in Reynolds number is accomplished by changing the stagnation pressure from about 1/4 atmosphere to 4 atmospheres, and the variation in Mach number is obtained by interchanging nozzle blocks which form test sections approximately 9 inches square.

The investigation was made at a Mach number of 2.91 and the Reynolds number, based on maximum model diameter, varied from 0.44×10^6 to 1.76×10^6 . The oscillation frequencies were such that the reduced-frequency parameter k varied from approximately 0.0045 to 0.015, depending on the moment of inertia and static stability of each model. Schlieren photographs were taken of the flow about each model for all the test conditions.

Changes in angle of attack from 0° to 14.10° were achieved by setting the sting support at various angles between 0° and 15° . The magnitude of the nosedown pitching moment caused the model to trim out at a somewhat smaller angle of attack than the preset sting angle, and this initial trim deflection reduced the magnitude of the deflection available for the oscillation tests. For example for model 1, the

0371200 1030

03

maximum amplitude of the oscillation about an angle of attack of 0° was 3.15° . At a sting angle of 10° , however, the nosedown pitching moment caused the model to trim out at 8.35° and thus reduced the initial oscillation amplitude to approximately 1.43° .

REDUCTION OF DATA

The static-stability parameter $(C_{m_{\alpha, \omega}} - k^2 C_{m_{\dot{q}, \omega}})$ and the damping-in-pitch parameter $(C_{m_{q, \omega}} + C_{m_{\dot{\alpha}, \omega}})$ were determined from the frequency of motion and rate of damping by the following equations obtained from reference 9:

$$C_{m_{\alpha, \omega}} - k^2 C_{m_{\dot{q}, \omega}} = - \frac{4\pi^2 I}{(P^2)_{\text{wind on } q_\infty \text{ Ad}}} + \frac{K}{q_\infty \text{ Ad}} \quad (1)$$

$$C_{m_{q, \omega}} + C_{m_{\dot{\alpha}, \omega}} = \frac{-2.772 IV}{q_\infty \text{ Ad}^2} \frac{1}{(t_{1/2})_{\text{aerodynamic}}} \quad (2)$$

where

$$I = \frac{(KP^2)_{\text{wind off}}}{4\pi^2}$$

and is obtained from the wind-off record. Inasmuch as there was some variation of the flexure spring constant K with axial load, it was necessary to take this variation into account when computing

$$C_{m_{\alpha, \omega}} - k^2 C_{m_{\dot{q}, \omega}}.$$

Previous experience had shown the internal damping of the crossed flexures to be a function of amplitude. A data-reduction method was set up in which the internal damping was subtracted from each cycle of wind-on record in accordance with this consideration. This method also minimized frequency effects on the damping.

The amplitude of oscillation, corrected for cross-pivot damping, was plotted against time on semilogarithmic paper. The period and time to damp to one-half amplitude were read from these plots. These data were used in equations (1) and (2) to calculate the static-stability and damping-in-pitch parameters. The range of amplitudes used in

defining the wind-on and wind-off decay curves was from the maximum initial amplitude down to several cycles beyond one-half of the maximum amplitude for each model.

The effect of amplitude of oscillation could be obtained by using different portions of the oscillation envelope to measure the time to damp to one-half amplitude ($t_{1/2}$). Thus, for model 1, the data at α_m of 0° were used to determine the damping for θ_0 of 2.43° , 1.43° , and 1.00° corresponding to the maximum amplitudes obtained at the larger angles of attack for a Reynolds number of 0.44×10^6 . The data at α_m of 4.45° were handled in the same manner to obtain a measure of the damping for θ_0 of 1.43° and 1.00° ; and, similarly, the data at α_m of 8.35° , for θ_0 of 1.00° . Thus, both the variation of damping with decrease in amplitude θ_0 at each angle of attack and the variation in damping with increase in angle of attack α_m for specific amplitudes could be evaluated. This procedure was applied to each model tested.

The experimental values shown in table II are the average $C_{m_{q,\omega}} + C_{m_{\dot{\alpha},\omega}}$ and $C_{m_{\alpha,\omega}} - k^2 C_{m_{q,\omega}}$ values for three runs. The average $C_{m_{q,\omega}} + C_{m_{\dot{\alpha},\omega}}$ values varied approximately 5 percent from the value determined from each record. The maximum probable error in the calculation of $C_{m_{\alpha,\omega}} - k^2 C_{m_{q,\omega}}$ is estimated to be 10 percent.

RESULTS AND DISCUSSION

The results of this investigation are presented in table II and in figures 5 to 8. Figures 5 to 8 present typical schlieren photographs of the flow about the models at various angles of attack. The boundary-layer thickness and, for some of the supersonic-impact models, areas of separated flow are discernible. Table II presents the data of this investigation and the test conditions.

Newtonian calculations of the derivatives were obtained by the use of reference 7 and are presented in table II for easy comparison with measured derivatives. Derivatives were also calculated by the use of the combined first- and second-order theory for cones of reference 8. In these calculations, the total derivatives were approximated by the addition and subtraction in an appropriate way of the contribution of the various conical segments as was done in reference 7 by using Newtonian impact theory. Although no theoretical basis exists for

03171233 1:30

8

combining these derivatives in this manner, it was felt instructive to show the derivatives that were obtained. It is interesting to note that the stability derivatives calculated by using this method showed the decrease in damping with increase in Mach number which was obtained experimentally in reference 3. Use of this method results in a reasonable indication of the magnitude of the damping derivatives. The following table presents the calculated derivatives:

Model	C_{m_q}	C_{m_α}	$C_{m_q} + C_{m_{\dot{\alpha}}}$	C_{m_α}	$C_{m_q} + C_{m_{\dot{\alpha}}}$	C_{m_α}
	Newtonian theory		M = 2.91		M = 1.94	
			Combined first- and second-order cone theory			
1	-3.13	-0.27	-9.05	-0.16	-11.08	-0.30
2	-3.65	-.59	-7.77	-.48	-10.22	-.61
3	-5.67	-1.08	-7.33	-1.01	-8.73	-1.07
5	-3.36	-.17	-9.27	-.07	-11.28	-.21
6	-5.91	-.98	-7.56	-.92	-8.93	-.99
7	-2.64	-1.05	-3.75	-1.00	-4.84	-1.01
8	-4.30	-1.00	-5.14	-.78	-8.27	-.95
9	-.42	-.13				
10	-.29	-.16				
11	-.21	-.15				

The test data showed that the blunt cone and all the cylinder-flare models were dynamically and statically stable. Although the manned reentry capsule models also were generally dynamically and statically stable, the values of damping were much smaller than those for the cylinder-flare models. Only model 9 at the largest angle of attack and the lowest dynamic pressure had unfavorable damping.

L
1
3
4
3

A comparison of the data at 0° angle of attack with the data presented in reference 3 shows generally good agreement for the static-stability parameters $(C_{m_{\alpha,\omega}} - k^2 C_{m_{q,\omega}})$ determined from the two tests under identical test conditions but with different model supports. Agreement with $C_{m_{\alpha}}$ data presented in reference 2 also is generally good at comparable Reynolds numbers. The following table presents these comparisons:

Model	$C_{m_{\alpha,\omega}} - k^2 C_{m_{q,\omega}}$					$C_{m_{\alpha}}$
	Present test at $R =$		From ref. 3 at $R =$			From ref. 2 at $R = 1.30 \times 10^6$
	0.44×10^6	0.88×10^6	0.44×10^6	0.88×10^6	1.32×10^6	
1	-0.44	-0.39	-0.47	-0.35	-0.37	-0.15
2	-.58	-.51			-.49	-.48
3	-1.09	-.68	-1.05	-.71	-.68	-.72
4	-.39	-.36	-.44	-.32	-.33	
5	-.39	-.26	-.39	-.28	-.29	
6	-1.13	-.60		-.60	-.62	-.69
7	-.34	-.22	-.36	-.35	-.38	

For the damping derivative, however, the agreement of the data herein with the data presented in reference 3 was good for some of the models and poor for others. The different interference effects of the two support systems are believed responsible for the poor agreement between the two sets of data for some of the models. The two side-by-side 1/4-inch struts used on the model support for the tests of reference 3 evidently created interference effects which were different from those created by the single 1/4-inch support strut used in the present tests.

037103000000

0

Typical damping results for model 1 are as follows:

θ_o , deg	$C_{m_{q,\omega}} + C_{m_{\dot{\alpha},\omega}}$ for $R = 0.44 \times 10^6$ and $\alpha_m =$				θ_o , deg	$C_{m_{q,\omega}} + C_{m_{\dot{\alpha},\omega}}$ for $R = 0.88 \times 10^6$ and $\alpha_m =$		
	0°	4.45°	8.35°	11.25°		0°	3.90°	7.60°
3.15	-7.11				3.08	-7.24		
2.43	-5.59	-6.85			2.05	-6.79	-7.51	
1.43	-4.61	-3.98	-5.31		1.38	-5.80	-5.94	-5.30
1.00	-4.83	-3.62	-3.75	-4.52				

These data and the data in table II for models 1 to 8 show that the damping generally decreased with decrease in oscillation amplitude at the lower angles of attack. It is interesting to observe that the damping obtained for the initial amplitudes at the various angles of attack ($C_{m_{q,\omega}} + C_{m_{\dot{\alpha},\omega}} = -7.11, -6.85, -5.31, \text{ and } -4.52$) showed the same trend as was found for the variation of damping with amplitude at an angle of attack of 0° and thus indicated that the decrease in amplitude was probably primarily responsible for the decrease in damping. (Compare with data at $\alpha_m = 0^\circ$.)

The variation of damping with angle of attack for the lowest Reynolds number was inconsistent in that for some models the damping decreased and then increased as the angle of attack increased (see data for models 1 and 7) whereas for other models the reverse was true (see data for models 3 and 6). At the higher Reynolds number these erratic variations with angle of attack tended to disappear.

For the blunt-faced reentry capsule models, the angle of attack and amplitude effects were generally similar to those for models 1 to 8; that is, a decrease in amplitude decreased the damping and angle-of-attack effects were erratic.

The data in table II also showed that there was no apparent effect of oscillation amplitude on the static-stability parameter. An increase in angle of attack, however, generally increased this parameter.

CONCLUDING REMARKS

L
1
3
4
3

An experimental investigation has been made at a Mach number of 2.91 to determine the damping in pitch and static stability of blunt cone-cylinder-flare models and manned reentry capsule models. The tests were made at angles of attack from 0° to 14.10° and at initial amplitudes from 0.82° to 3.23° . It was found in the investigation that all the models had favorable damping-in-pitch and static-stability parameters and that the damping generally decreased as the amplitude of oscillation decreased at the lower angles of attack. The variation of the damping with increase in angle of attack, however, showed no consistent trends, but decreased and then increased with angle of attack for some models but not for others. These erratic variations tended to become smaller or disappear at the higher Reynolds number. The static-stability parameter was unaffected by decreases in oscillation amplitude but generally increased with increase in angle of attack.

Langley Research Center,

National Aeronautics and Space Administration,
Langley Field, Va., March 29, 1961.



REFERENCES

1. Gregory, Donald T., and Carraway, Ausley B.: An Investigation at Mach Numbers From 1.47 to 2.87 of Static Stability Characteristics of Nine Nose Cones Designed for Supersonic Impact Velocities. NASA TM X-69, 1959.
2. Swihart, John M.: Static Stability Investigation of Supersonic-Impact Ballistic Reentry Shapes at Mach Numbers of 2.55 and 3.05. NASA MEMO 5-27-59L, 1959.
3. Fletcher, Herman S., and Wolhart, Walter D.: Damping in Pitch and Static Stability of Supersonic Impact Nose Cones, Short Blunt Subsonic Impact Nose Cones, and Manned Reentry Capsules at Mach Numbers From 1.93 to 3.05. NASA TM X-347, 1960.
4. Fletcher, Herman S.: The Damping in Pitch and Static Stability of Six Supersonic-Impact Ballistic Configurations and Three High-Drag Reentry Capsules at a Mach Number of 6.83. NASA TM X-349, 1961.
5. Reese, David E., Jr., and Wehrend, William R., Jr.: An Investigation of the Static and Dynamic Aerodynamic Characteristics of a Series of Blunt-Nosed Cylinder-Flare Models at Mach Numbers From 0.65 to 2.20. NASA TM X-110, 1960.
6. Beam, Benjamin H., and Hedstrom, C. Ernest: The Damping in Pitch of Bluff Bodies at Mach Numbers From 2.5 to 3.5. NASA TM X-90, 1959.
7. Fisher, Lewis R.: Equations and Charts for Determining the Hypersonic Stability Derivatives of Combinations of Cone Frustums Computed by Newtonian Impact Theory. NASA TN D-149, 1959.
8. Tobak, Murray, and Wehrend, William R.: Stability Derivatives of Cones at Supersonic Speeds. NACA TN 3788, 1956.
9. Campbell, John P., and Mathews, Ward O.: Experimental Determination of the Yawing Moment Due to Yawing Contributed by the Wing, Fuselage, and Vertical Tail of a Midwing Model. NACA WR L-387, 1943. (Formerly NACA ARR 3F28.)

L
1
3
4
3

SECRETED

TABLE I.- MASS CHARACTERISTICS OF MODELS

Model	Weight, lb	I, slug-ft ²
1	0.442	0.0002860
2	.435	.0003579
3	.373	.0002710
4	.493	.0004127
5	.427	.0002880
6	.370	.0002800
7	.343	.0002532
8	.336	.0003687
9	.394	.0000630
10	.406	.0000787
11	.337	.0000544

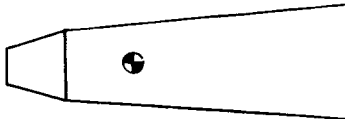
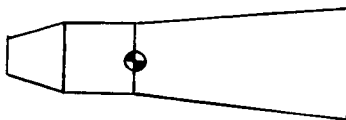
SECRETED

037 [REDACTED] 30

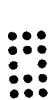
8

TABLE II.- EXPERIMENTAL RESULTS, NEWTONIAN THEORY RESULTS,
AND TEST CONDITIONS

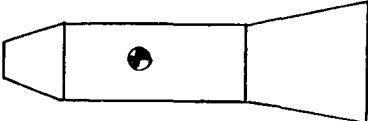
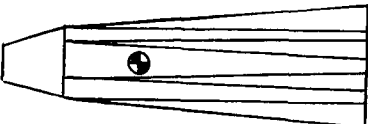
$$[M = 2.91]$$

R	q_∞ , lb/sq ft	α_s , deg	α_m , deg	θ_o , deg	$C_{m_{q,\omega}} + C_{m_{\dot{\alpha},\omega}}$	$C_{m_{\alpha,\omega}} - k^2 C_{m_{\dot{q},\omega}}$	k
 Model 1							
0.44×10^6	409	$\left\{ \begin{array}{l} 0 \\ 5 \\ 10 \\ 12.5 \end{array} \right.$	$\left\{ \begin{array}{l} 0 \\ 4.45 \\ 8.35 \\ 11.25 \end{array} \right.$	$\left\{ \begin{array}{l} 3.15 \\ 2.43 \\ 1.43 \\ 1.00 \end{array} \right.$ $\left\{ \begin{array}{l} 2.43 \\ 1.43 \\ 1.00 \end{array} \right.$ $\left\{ \begin{array}{l} 1.43 \\ 1.00 \end{array} \right.$ $\left\{ \begin{array}{l} 1.00 \end{array} \right.$	$\left\{ \begin{array}{l} -7.11 \\ -5.59 \\ -4.66 \\ -4.53 \end{array} \right.$ $\left\{ \begin{array}{l} -6.85 \\ -3.98 \\ -3.62 \end{array} \right.$ $\left\{ \begin{array}{l} -5.31 \\ -3.75 \end{array} \right.$ $\left\{ \begin{array}{l} -4.52 \end{array} \right.$	$\left\{ \begin{array}{l} -0.44 \\ -0.64 \\ -1.00 \\ -1.28 \end{array} \right.$	0.00542 $.00558$ $.00586$ $.00606$
$.88 \times 10^6$	783	$\left\{ \begin{array}{l} 0 \\ 5 \\ 10 \end{array} \right.$	$\left\{ \begin{array}{l} 0 \\ 3.90 \\ 7.60 \end{array} \right.$	$\left\{ \begin{array}{l} 3.08 \\ 2.05 \\ 1.38 \end{array} \right.$ $\left\{ \begin{array}{l} 2.05 \\ 1.38 \end{array} \right.$ $\left\{ \begin{array}{l} 1.38 \end{array} \right.$	$\left\{ \begin{array}{l} -7.24 \\ -6.79 \\ -5.80 \end{array} \right.$ $\left\{ \begin{array}{l} -7.51 \\ -5.94 \end{array} \right.$ $\left\{ \begin{array}{l} -5.30 \end{array} \right.$	$\left\{ \begin{array}{l} -.39 \\ -.52 \\ -.73 \end{array} \right.$	$.00564$ $.00584$ $.00613$
Newtonian theory					$C_{m_q} = -3.13$	$C_{m_\alpha} = -0.27$	
 Model 2							
0.44×10^6	411	$\left\{ \begin{array}{l} 0 \\ 5 \\ 10 \end{array} \right.$	$\left\{ \begin{array}{l} 0 \\ 3.90 \\ 8.65 \end{array} \right.$	$\left\{ \begin{array}{l} 3.06 \\ 2.30 \\ 1.18 \end{array} \right.$ $\left\{ \begin{array}{l} 2.30 \\ 1.18 \end{array} \right.$ $\left\{ \begin{array}{l} 1.18 \end{array} \right.$	$\left\{ \begin{array}{l} -7.53 \\ -6.60 \\ -3.64 \end{array} \right.$ $\left\{ \begin{array}{l} -6.45 \\ -4.80 \end{array} \right.$ $\left\{ \begin{array}{l} -4.59 \end{array} \right.$	$\left\{ \begin{array}{l} -0.58 \\ -.71 \\ -1.05 \end{array} \right.$	0.00499 $.00507$ $.00530$
$.88 \times 10^6$	785	$\left\{ \begin{array}{l} 0 \\ 5 \\ 7.5 \end{array} \right.$	$\left\{ \begin{array}{l} 0 \\ 3.25 \\ 5.10 \end{array} \right.$	$\left\{ \begin{array}{l} 2.95 \\ 1.70 \\ .94 \end{array} \right.$ $\left\{ \begin{array}{l} .94 \\ 1.70 \end{array} \right.$ $\left\{ \begin{array}{l} .94 \end{array} \right.$	$\left\{ \begin{array}{l} -6.36 \\ -6.29 \\ -5.29 \end{array} \right.$ $\left\{ \begin{array}{l} -6.22 \\ -4.63 \end{array} \right.$ $\left\{ \begin{array}{l} -5.80 \end{array} \right.$	$\left\{ \begin{array}{l} -.51 \\ -.66 \\ -.76 \end{array} \right.$	$.00517$ $.00538$ $.00550$
Newtonian theory					$C_{m_q} = -3.65$	$C_{m_\alpha} = -0.59$	

L-1343

TABLE II.- EXPERIMENTAL RESULTS, NEWTONIAN THEORY RESULTS,
AND TEST CONDITIONS - Continued

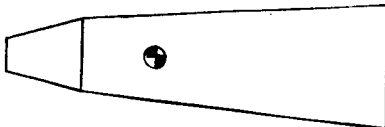
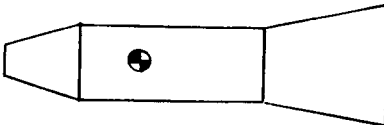
$$[M = 2.91]$$

R	q_∞ , lb/sq ft	α_s , deg	α_m , deg	θ_o , deg	$C_{mq,\omega} + C_{m\dot{\alpha},\omega}$	$C_{m\alpha,\omega} - k^2 C_{mq,\omega}$	k
 Model 3							
0.44×10^6	401	$\begin{cases} 0 \\ 5 \\ 7.5 \end{cases}$	$\begin{cases} 0 \\ 3.50 \\ 5.00 \end{cases}$	$\begin{cases} \begin{cases} 2.96 \\ 2.15 \\ 1.57 \end{cases} \\ \begin{cases} 2.15 \\ 1.57 \end{cases} \\ 1.57 \end{cases}$	$\begin{cases} \begin{cases} -5.62 \\ -3.97 \\ -2.53 \end{cases} \\ \begin{cases} -7.97 \\ -8.09 \end{cases} \\ -5.93 \end{cases}$	$\begin{cases} -1.09 \\ -.73 \\ -.98 \end{cases}$	$\begin{cases} 0.00614 \\ .00590 \\ .00603 \end{cases}$
$.88 \times 10^6$	782	$\begin{cases} 0 \\ 5 \end{cases}$	$\begin{cases} 0 \\ 3.20 \end{cases}$	$\begin{cases} \begin{cases} 2.94 \\ 1.72 \\ 1.57 \end{cases} \\ \begin{cases} 1.72 \\ 1.57 \end{cases} \end{cases}$	$\begin{cases} \begin{cases} -7.32 \\ -6.46 \\ -6.46 \end{cases} \\ \begin{cases} -7.12 \\ -7.12 \end{cases} \end{cases}$	$\begin{cases} -.68 \\ -.76 \end{cases}$	$\begin{cases} .00623 \\ .00633 \end{cases}$
Newtonian theory					$C_{mq} = -5.67$	$C_{m\alpha} = -1.08$	
 Model 4							
0.44×10^6	408	$\begin{cases} 0 \\ 5 \\ 0 \end{cases}$	$\begin{cases} 0 \\ 4 \\ 7.55 \end{cases}$	$\begin{cases} \begin{cases} 2.75 \\ 2.30 \\ 1.43 \end{cases} \\ \begin{cases} 2.30 \\ 1.43 \end{cases} \\ .82 \end{cases}$	$\begin{cases} \begin{cases} -5.64 \\ -5.03 \\ -4.35 \end{cases} \\ \begin{cases} -5.48 \\ -4.09 \end{cases} \\ -4.55 \end{cases}$	$\begin{cases} -0.39 \\ -.74 \\ -1.12 \end{cases}$	$\begin{cases} 0.00448 \\ .00471 \\ .00495 \end{cases}$
$.88 \times 10^6$	782	$\begin{cases} 0 \\ 5 \end{cases}$	$\begin{cases} 0 \\ 3.35 \end{cases}$	$\begin{cases} \begin{cases} 2.62 \\ 1.73 \end{cases} \\ 1.73 \end{cases}$	$\begin{cases} \begin{cases} -5.85 \\ -4.19 \end{cases} \\ -4.55 \end{cases}$	$\begin{cases} -.36 \\ -.84 \end{cases}$	$\begin{cases} .00467 \\ .00522 \end{cases}$

L-1343

TABLE II.- EXPERIMENTAL RESULTS, NEWTONIAN THEORY RESULTS,
AND TEST CONDITIONS - Continued

$$[M = 2.91]$$

R	q_∞ , lb/sq ft	α_s , deg	α_m , deg	θ_o , deg	$C_{m_{q,\omega}} + C_{m_{\dot{\alpha},\omega}}$	$C_{m_{\alpha,\omega}} - k^2 C_{m_{\dot{q},\omega}}$	k	
<div></div> <div>Model 5</div>								
0.44×10^6	408	{	0	0	{ 2.18 2.02 1.45 1.17	{ -5.71 -5.08 -4.92 -4.46	-0.39	0.00538
			5	4.45	{ 2.02 1.45 1.17	{ -6.60 -7.00 -6.76		
			10	8.75	{ 1.45 1.17	{ -5.29 -4.70		
			12.5	10.95	1.17	-5.73		
$.88 \times 10^6$	786	{	0	0	{ 3.14 2.24 1.10	{ -7.95 -7.64 -6.56	-.26	.00545
			6	5	{ 2.24 1.10	{ -7.21 -5.30		
			10	8.35	1.10	-5.23		
Newtonian theory					$C_{m_q} = -3.36$	$C_{m_\alpha} = -0.17$		
<div></div> <div>Model 6</div>								
0.44×10^6	408	{	0	0	{ 3.00 2.10 1.10	{ -4.96 -3.49 -1.04	-1.13	0.00610
			5	3.80	{ 2.10 1.10	{ -9.10 -5.02		
$.88 \times 10^6$	782	{	0	0	{ 3.00 1.80 1.00	{ -8.43 -7.42 -5.85	-.60	.00601
			5	3.50	{ 1.80 1.00	{ -7.92 -6.86		
			7.5	5.90	1.00	-6.97		
Newtonian theory					$C_{m_q} = -5.91$	$C_{m_\alpha} = -0.98$		

$$[M = 2.91]$$

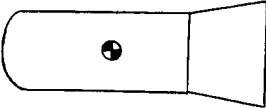
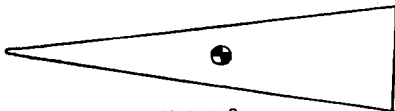
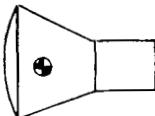
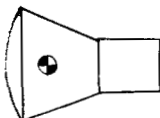
R	q_∞ , lb/sq ft	α_s , deg	α_m , deg	θ_o , deg	$C_{mq,w} + C_{m\alpha,w}$	$C_{m\alpha,w} - k^2 C_{mq,w}$	k
 <p style="text-align: center;">Model 7</p>							
0.44×10^6	411	$\left\{ \begin{array}{l} 0 \\ 5 \\ 10 \end{array} \right.$	$\left\{ \begin{array}{l} 0 \\ 3.85 \\ 8.75 \end{array} \right.$	$\left\{ \begin{array}{l} 3.17 \\ 2.75 \\ 2.42 \\ 2.10 \\ 1.00 \\ 2.75 \\ 2.42 \\ 2.10 \\ 1.00 \\ 2.42 \\ 2.10 \\ 1.00 \end{array} \right.$	$\left\{ \begin{array}{l} -3.63 \\ -3.70 \\ -3.72 \\ -3.62 \\ -2.56 \\ -2.70 \\ -2.96 \\ -2.95 \\ -1.86 \\ -4.56 \\ -5.81 \\ -2.03 \end{array} \right.$	$\left\{ \begin{array}{l} -0.34 \\ -.34 \\ -.34 \end{array} \right.$	$\left\{ \begin{array}{l} 0.00566 \\ .00566 \\ .00566 \end{array} \right.$
$.88 \times 10^6$	785	$\left\{ \begin{array}{l} 0 \\ 5 \\ 10 \end{array} \right.$	$\left\{ \begin{array}{l} 0 \\ 4.05 \\ 8.10 \end{array} \right.$	$\left\{ \begin{array}{l} 3.14 \\ 2.57 \\ 1.48 \\ 2.57 \\ 1.48 \\ 1.48 \end{array} \right.$	$\left\{ \begin{array}{l} -4.11 \\ -4.08 \\ -3.40 \\ -3.67 \\ -3.09 \\ -2.22 \end{array} \right.$	$\left\{ \begin{array}{l} -.22 \\ -.39 \\ -.65 \end{array} \right.$	$\left\{ \begin{array}{l} .00566 \\ .00593 \\ .00632 \end{array} \right.$
1.32×10^6	1,177	$\left\{ \begin{array}{l} 0 \\ 5 \end{array} \right.$	$\left\{ \begin{array}{l} 0 \\ 4.52 \end{array} \right.$	$\left\{ \begin{array}{l} 3.00 \\ 2.40 \\ 2.40 \end{array} \right.$	$\left\{ \begin{array}{l} -3.86 \\ -3.86 \\ -3.98 \end{array} \right.$	$\left\{ \begin{array}{l} -.27 \\ -.34 \end{array} \right.$	$\left\{ \begin{array}{l} .00583 \\ .00596 \end{array} \right.$
Newtonian theory					$C_{mq} = -2.64$	$C_{m\alpha} = -1.05$	
 <p style="text-align: center;">Model 8</p>							
0.44×10^6	411	$\left\{ \begin{array}{l} 0 \\ 5 \\ 8 \end{array} \right.$	$\left\{ \begin{array}{l} 0 \\ 4.15 \\ 6.35 \end{array} \right.$	$\left\{ \begin{array}{l} 3.20 \\ 2.16 \\ 1.55 \\ 2.16 \\ 1.55 \\ 1.55 \end{array} \right.$	$\left\{ \begin{array}{l} -5.78 \\ -4.52 \\ -3.64 \\ -6.90 \\ -4.70 \\ -6.64 \end{array} \right.$	$\left\{ \begin{array}{l} -1.01 \\ -1.02 \\ -1.09 \end{array} \right.$	$\left\{ \begin{array}{l} 0.00524 \\ .00518 \\ .00523 \end{array} \right.$
$.88 \times 10^6$	785	$\left\{ \begin{array}{l} 0 \\ 5 \end{array} \right.$	$\left\{ \begin{array}{l} 0 \\ 4.20 \end{array} \right.$	$\left\{ \begin{array}{l} 3.10 \\ 1.59 \\ 1.59 \end{array} \right.$	$\left\{ \begin{array}{l} -7.44 \\ -6.54 \\ -5.42 \end{array} \right.$	$\left\{ \begin{array}{l} -.83 \\ -1.09 \end{array} \right.$	$\left\{ \begin{array}{l} .00553 \\ .00573 \end{array} \right.$
1.32×10^6	1,177	$\left\{ \begin{array}{l} 0 \end{array} \right.$	$\left\{ \begin{array}{l} 0 \end{array} \right.$	$\left\{ \begin{array}{l} 2.30 \\ 1.56 \end{array} \right.$	$\left\{ \begin{array}{l} -8.34 \\ -8.34 \end{array} \right.$	$\left\{ \begin{array}{l} -.72 \end{array} \right.$	$\left\{ \begin{array}{l} .00574 \end{array} \right.$
1.76×10^6	1,570	$\left\{ \begin{array}{l} 0 \end{array} \right.$	$\left\{ \begin{array}{l} 0 \end{array} \right.$	$\left\{ \begin{array}{l} 1.64 \end{array} \right.$	$\left\{ \begin{array}{l} -7.06 \end{array} \right.$	$\left\{ \begin{array}{l} -.85 \end{array} \right.$	$\left\{ \begin{array}{l} .00639 \end{array} \right.$
Newtonian theory					$C_{mq} = -4.30$	$C_{m\alpha} = -1.00$	

TABLE II.- EXPERIMENTAL RESULTS, NEWTONIAN THEORY RESULTS,
AND TEST CONDITIONS - Continued

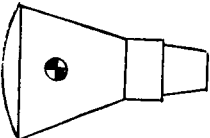
$$[M = 2.91]$$

R	q_∞ , lb/sq ft	α_s , deg	α_m , deg	θ_o , deg	$C_{m_{q,\omega}} + C_{m_{\alpha,\omega}}$	$C_{m_{\alpha,\omega}} - k^2 C_{m_{q,\omega}}$	k	
<div></div> <div>Model 9</div>								
0.55×10^6	401	{	0	0	{	{	-0.34	0.01418
			5	4.75	{			
		{	7.5	6.80	{	{	-0.42	.01454
			10	8.60	{			
1.10×10^6	780	{	0	0	{	{	-0.49	.01480
			5	3.65	{			
		{			{	{	-0.33	.01468
					{			
Newtonian theory					$C_{m_q} = -0.42$	$C_{m_\alpha} = -0.13$		
<div></div> <div>Model 10</div>								
0.55×10^6	401	{	0	0	{	{	-0.33	0.01270
			5	4.65	{			
		{	7.5	6.20	{	{	-0.42	.01304
			10	8.80	{			
1.10×10^6	779	{	0	0	{	{	-0.44	.01316
			5	4.40	{			
		{			{	{	-0.33	.01343
					{			
Newtonian theory					$C_{m_q} = -0.29$	$C_{m_\alpha} = -0.16$		

L-1343

TABLE II.- EXPERIMENTAL RESULTS, NEWTONIAN THEORY RESULTS,
AND TEST CONDITIONS - Concluded

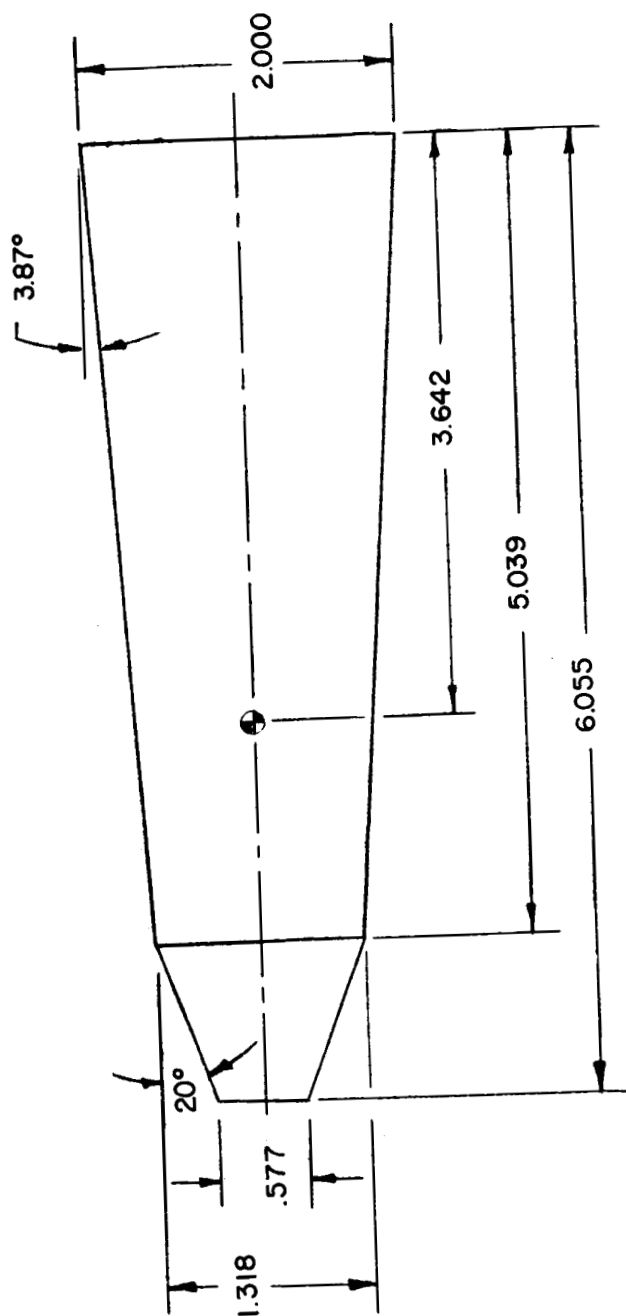
$$[M = 2.91]$$

R	q_∞ lb/sq ft	α_s , deg	α_m , deg	θ_o , deg	$C_{m_{q,\omega}} + C_{m_{\alpha,\omega}}$	$C_{m_{\alpha,\omega}} - k^2 C_{m_{q,\omega}}$	k
 <p>Model 11</p>							
0.495×10^6	408	0	0	$\begin{cases} 2.80 \\ 2.76 \\ 2.62 \\ 2.46 \\ 1.80 \end{cases}$	$\begin{cases} -0.22 \\ -.22 \\ -.21 \\ -.20 \\ -.13 \end{cases}$	-0.34	0.01352
		5	4.75	$\begin{cases} 2.76 \\ 2.62 \\ 2.46 \\ 1.80 \end{cases}$	$\begin{cases} -.09 \\ -.06 \\ -.06 \\ -.08 \end{cases}$	-.34	.01352
		10	9.90	$\begin{cases} 2.62 \\ 2.46 \\ 1.80 \end{cases}$	$\begin{cases} -.15 \\ -.15 \\ -.06 \end{cases}$	-.33	.01351
		15	14.10	$\begin{cases} 2.46 \\ 1.80 \end{cases}$	$\begin{cases} -.19 \\ -.12 \end{cases}$	-.33	.01349
$.99 \times 10^6$	782	0	0	$\begin{cases} 2.88 \\ 2.80 \\ 2.46 \\ 1.80 \end{cases}$	$\begin{cases} -.16 \\ -.16 \\ -.08 \\ -.01 \end{cases}$	-.33	.01391
		5	4.38	$\begin{cases} 2.80 \\ 2.46 \\ 1.80 \end{cases}$	$\begin{cases} -.11 \\ -.10 \\ -.14 \end{cases}$	-.34	.01392
1.48×10^6	1,177	0	0	$\begin{cases} 2.80 \\ 2.46 \\ 1.80 \end{cases}$	$\begin{cases} -.15 \\ -.10 \\ -.11 \end{cases}$	-.33	.01436
Newtonian theory					$C_{m_q} = -0.21$	$C_{m_\alpha} = -0.15$	

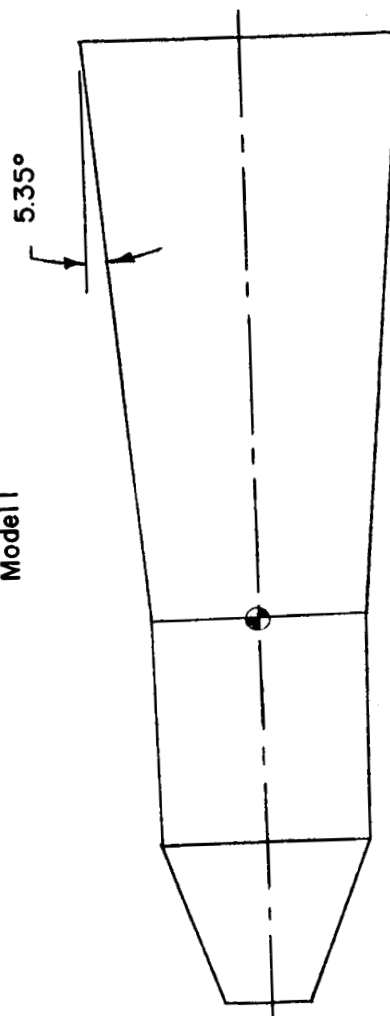
L-1343

CONFIDENTIAL

CONFIDENTIAL



Model 1



Model 2

Figure 1.- Drawings of models. All linear dimensions are in inches.

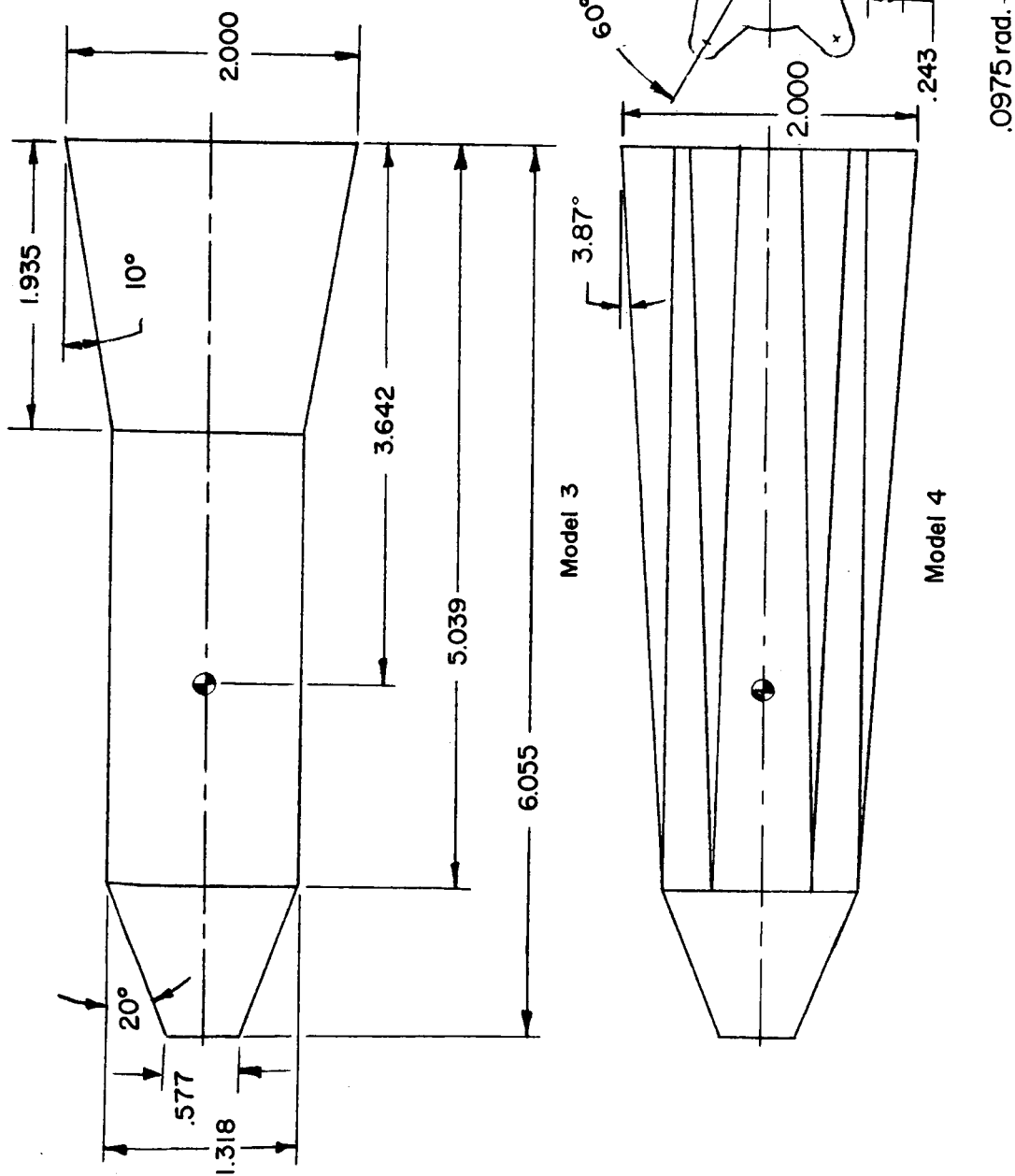


Figure 1.- Continued.

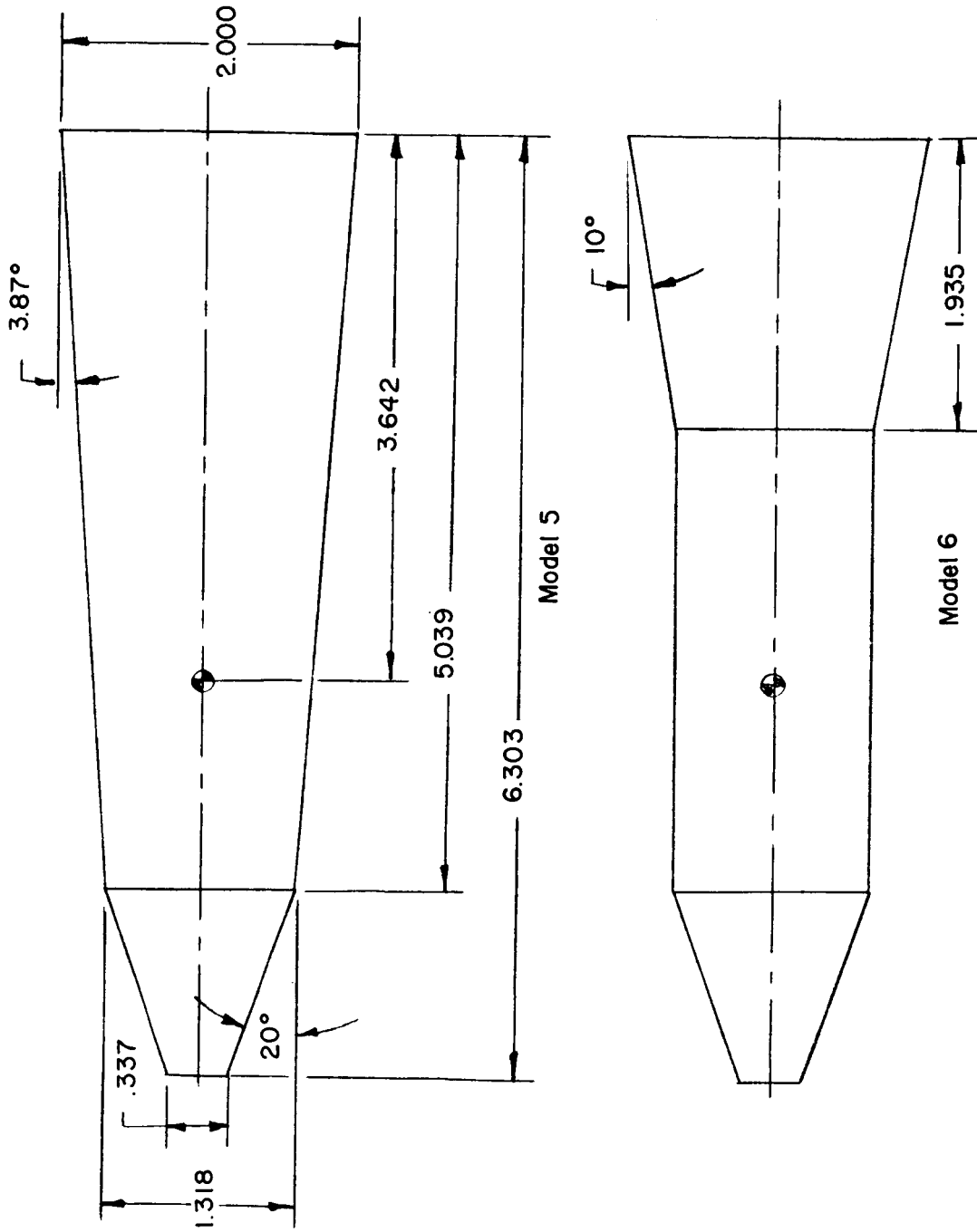


Figure 1.- Continued.

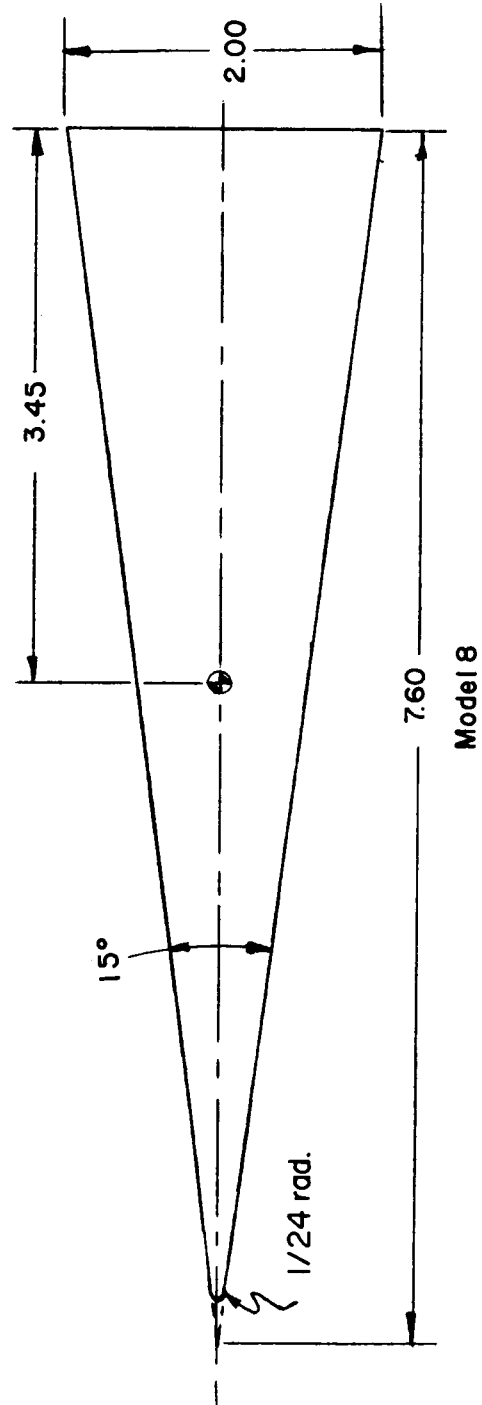
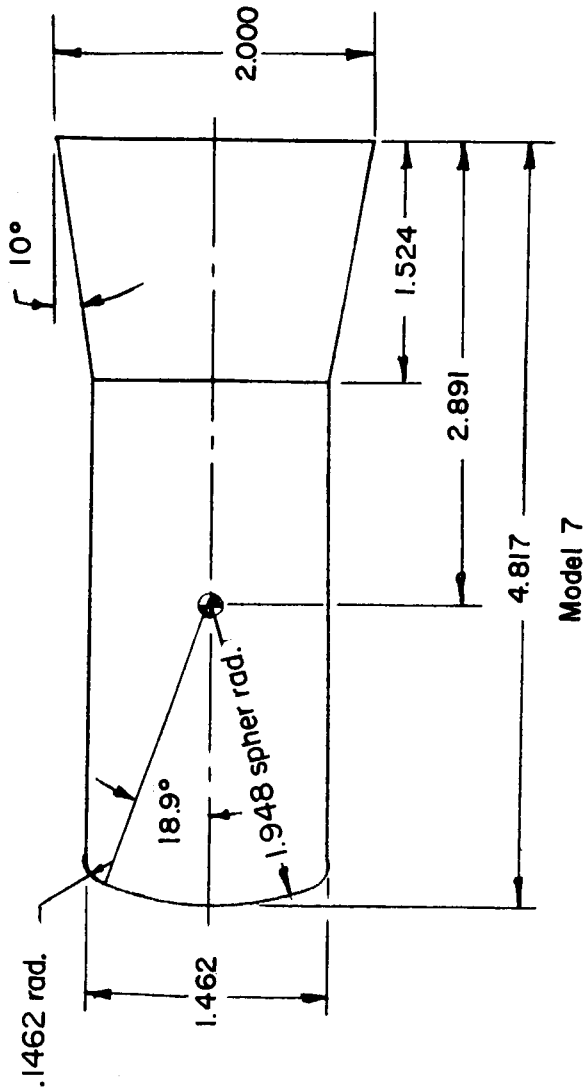
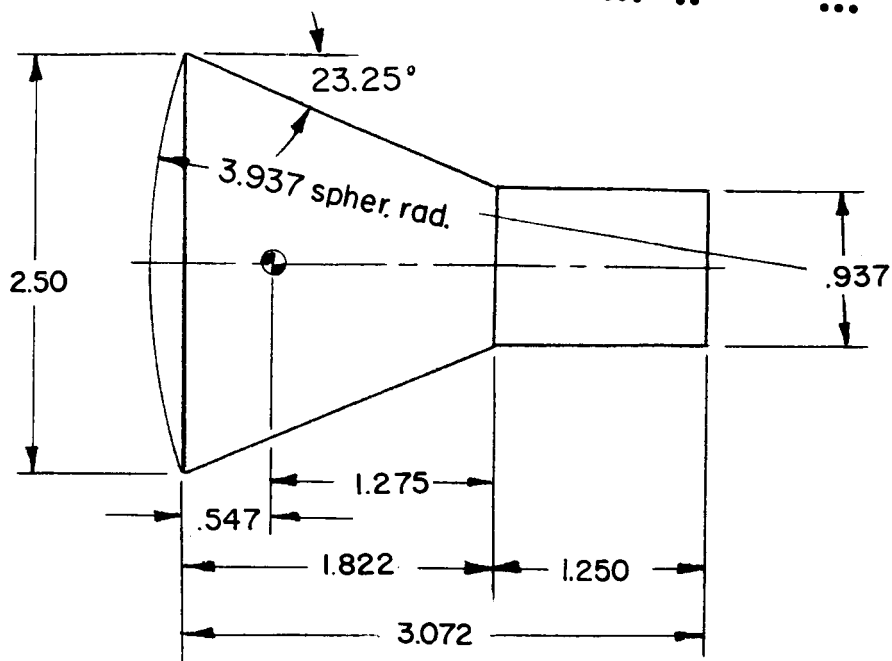
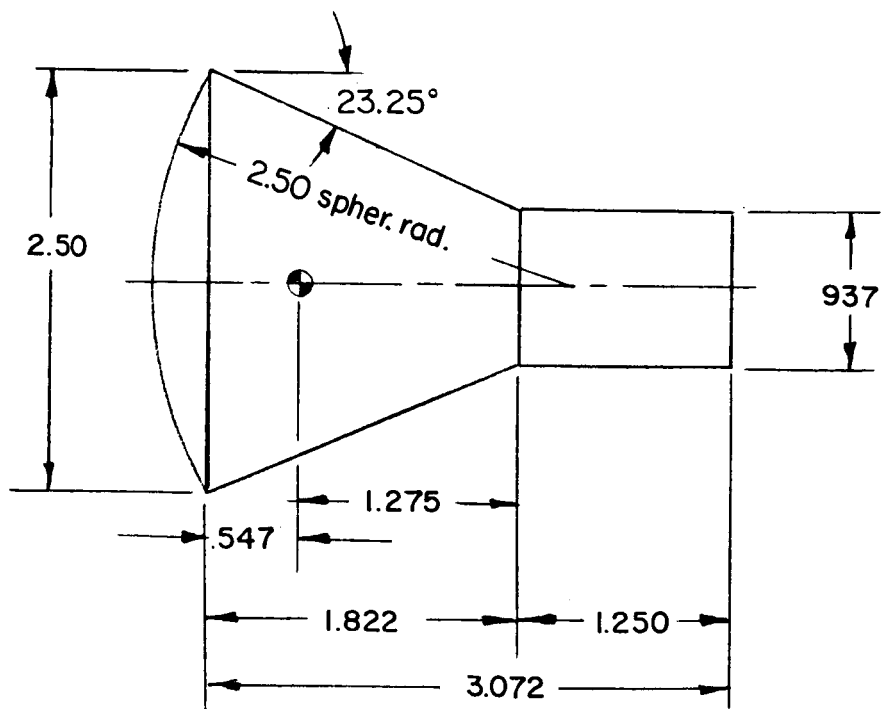


Figure 1.- Continued.



Model 9



Model 10

Figure 1.- Continued.

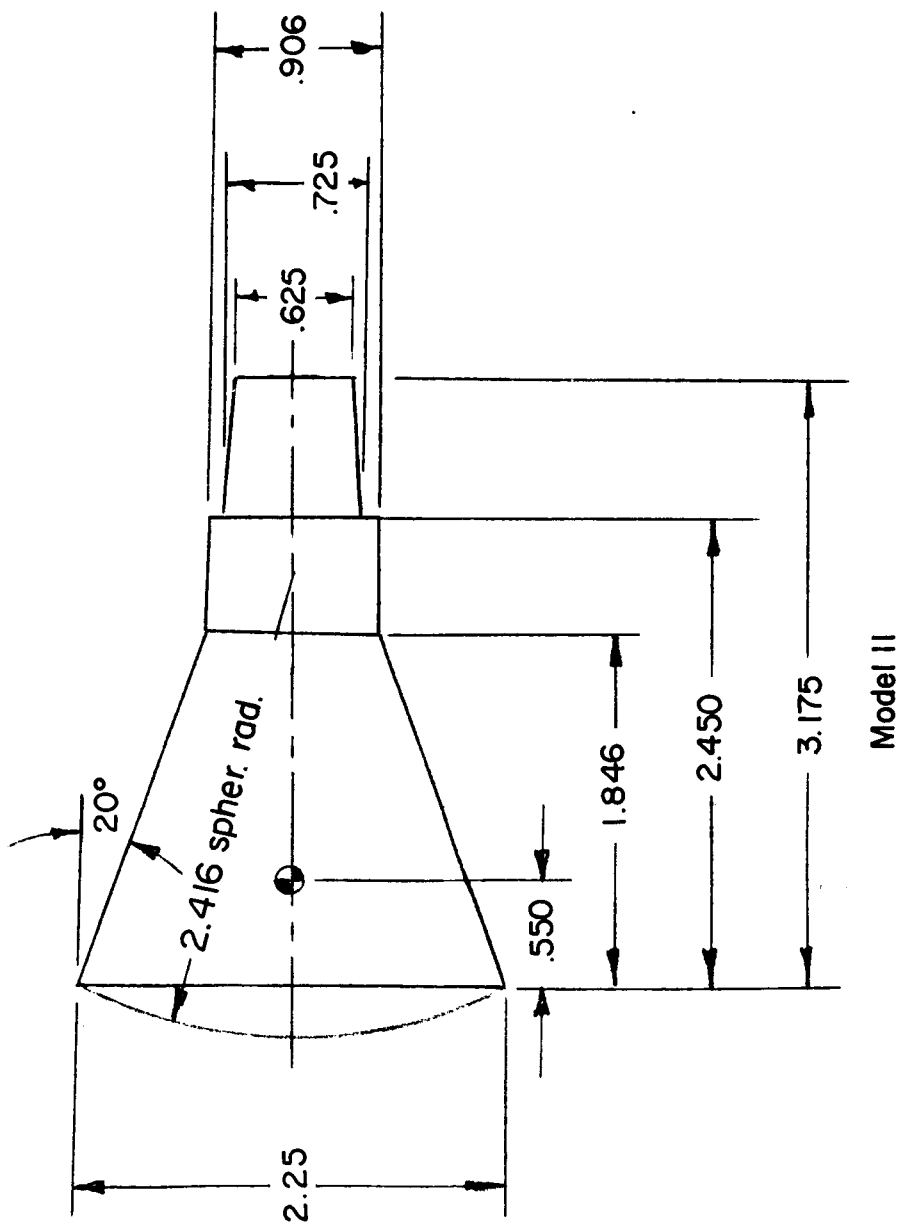


Figure 1.- Concluded.

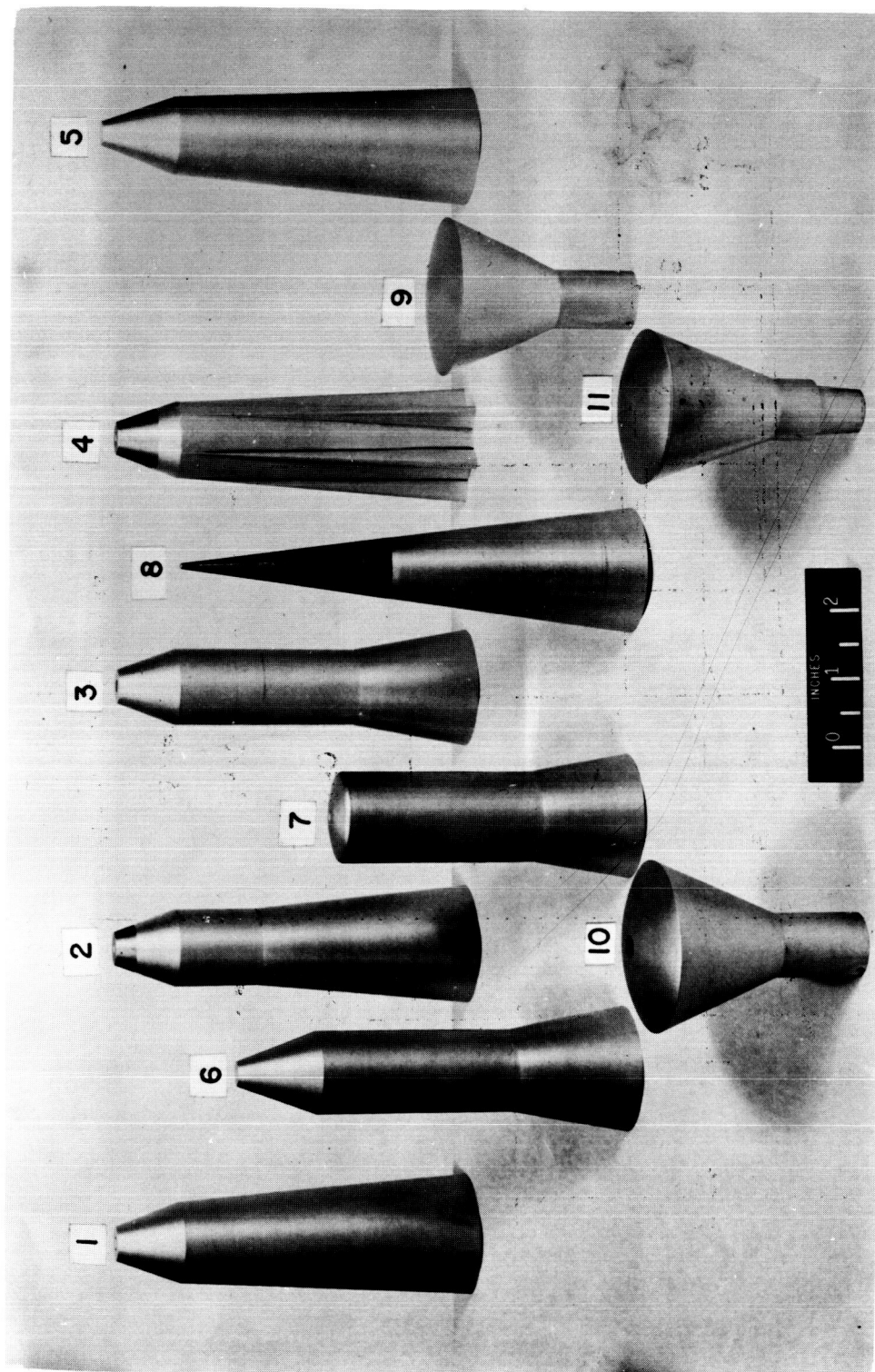


Figure 2.- Photograph of models. L-60-1965.1

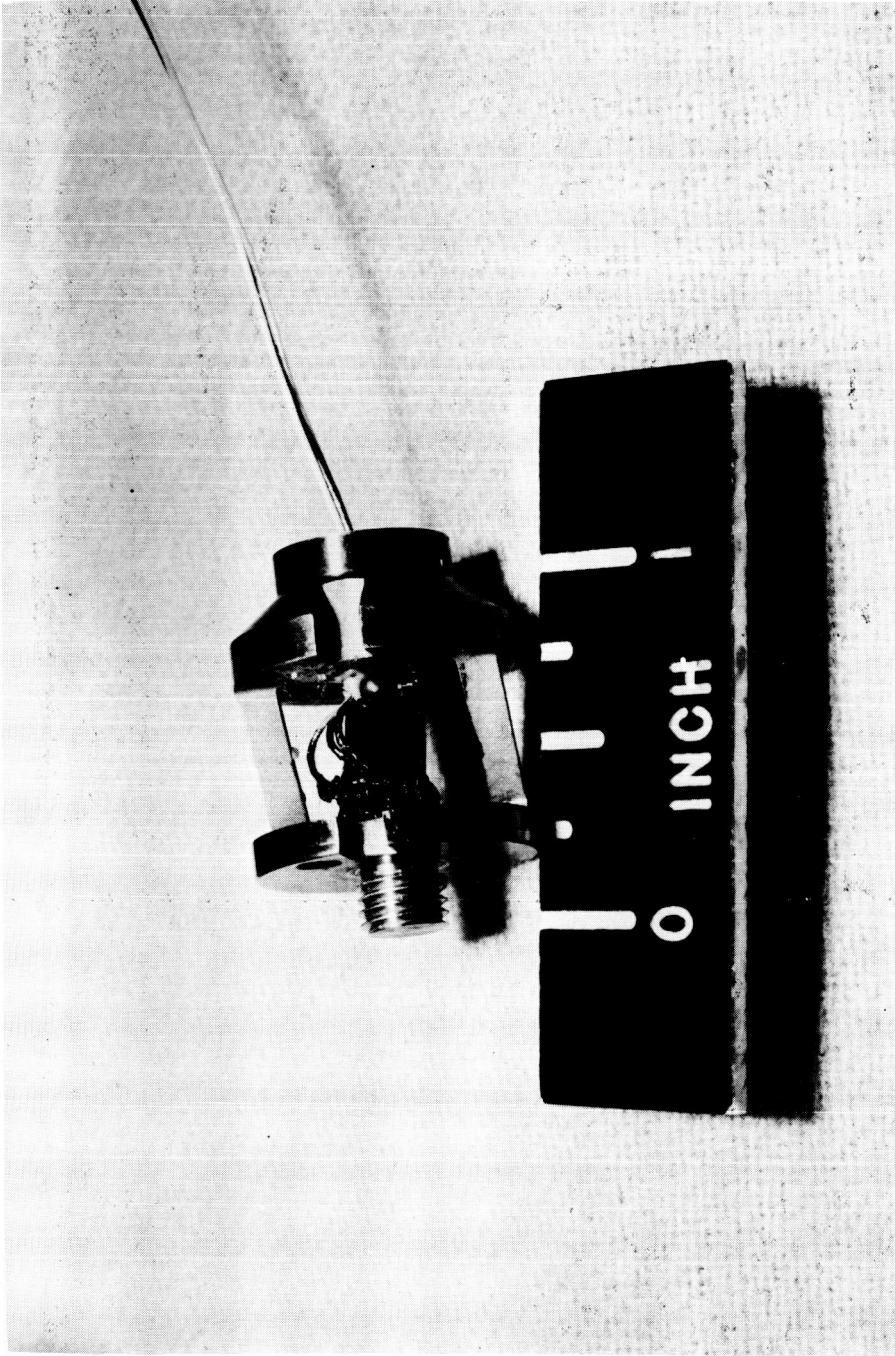
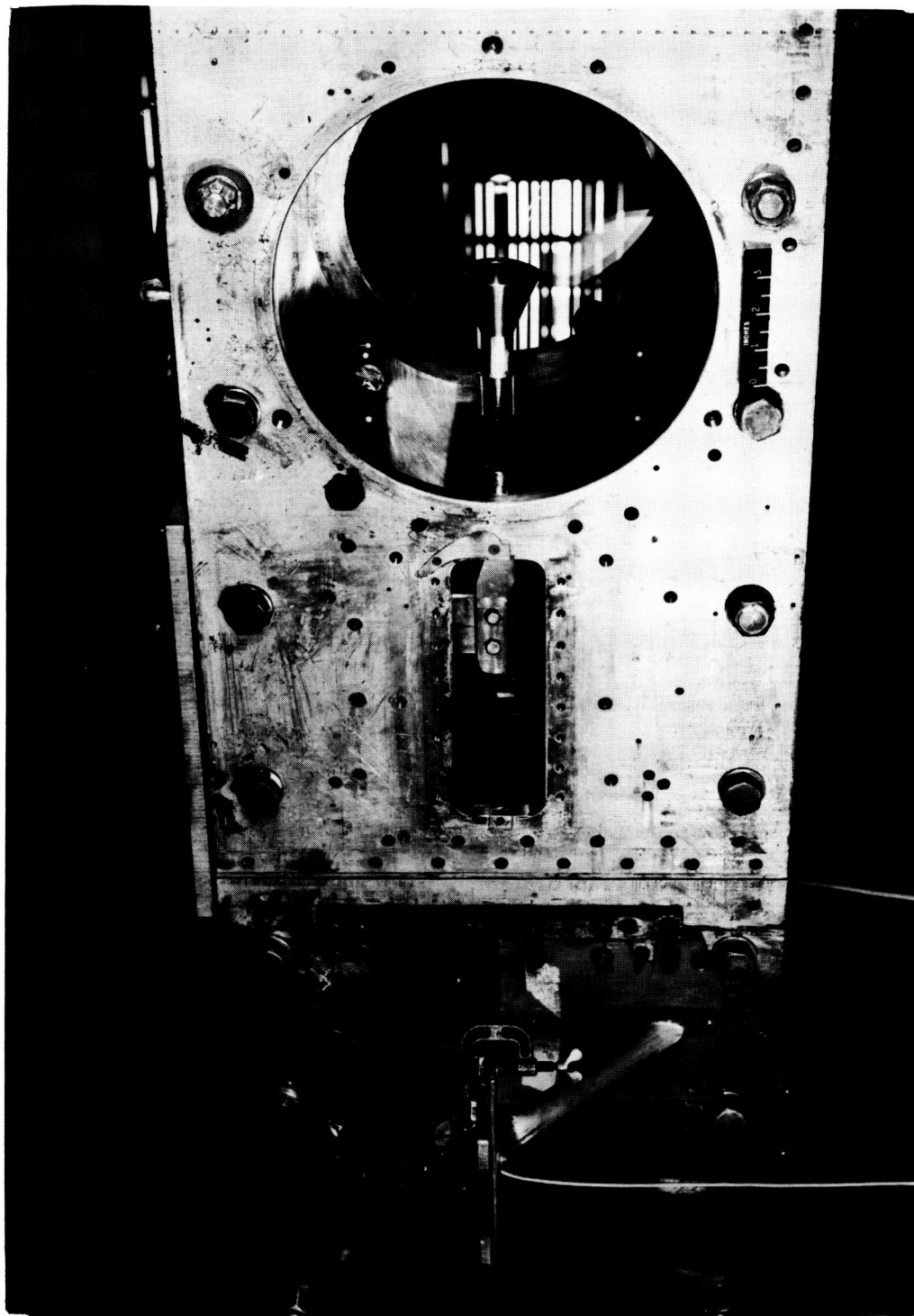


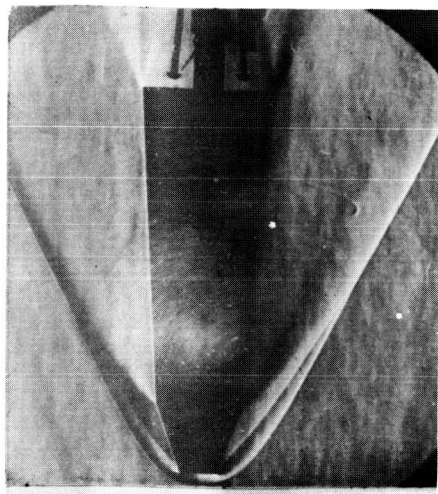
Figure 3.- Photograph of strain gage. L-58-1579

CONFIDENTIAL

CONFIDENTIAL



L-59-8070
Figure 4.- Photograph of model 10 mounted in Langley 9-inch supersonic tunnel.



$R = 0.44 \times 10^6$

$\alpha_m = 0^\circ$



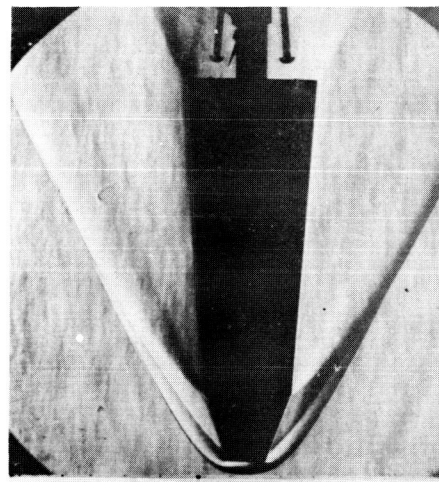
$R = 0.44 \times 10^6$

$\alpha_m = 4.45^\circ$



$R = 0.44 \times 10^6$

$\alpha_m = 8.35^\circ$



$R = 0.88 \times 10^6$

$\alpha_m = 0^\circ$



$R = 0.88 \times 10^6$

$\alpha_m = 3.90^\circ$



$R = 0.88 \times 10^6$

$\alpha_m = 7.60^\circ$

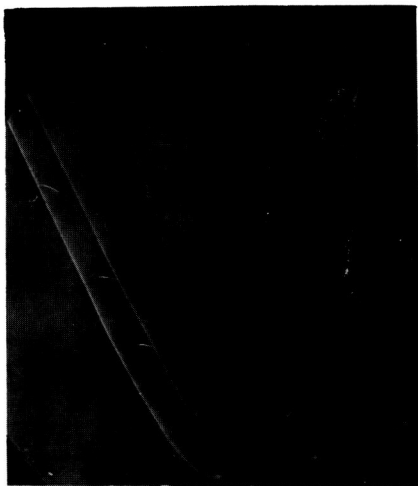
(a) Model 1.

L-61-1073

Figure 5.- Typical schlieren photographs of supersonic-impact models.

03712

03712



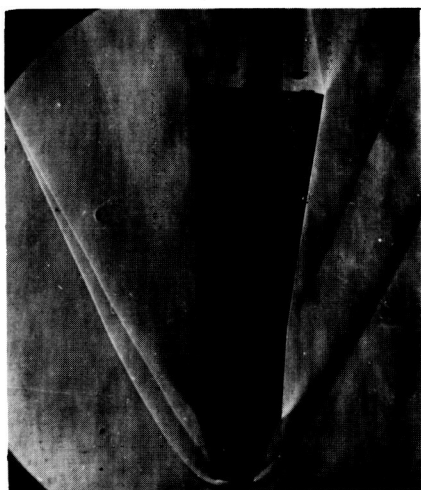
$R = 0.44 \times 10^6$ $\alpha_m = 8.65^\circ$



$\alpha_m = 5.10^\circ$

$R = 0.88 \times 10^6$

L-61-1074

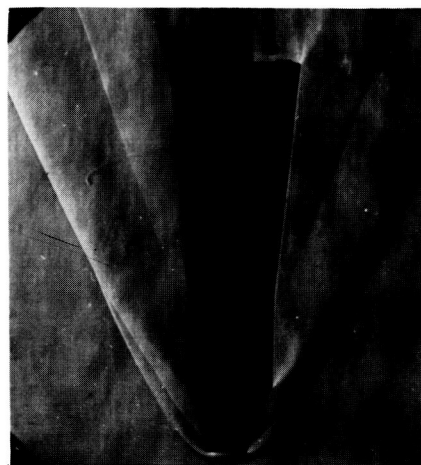


$R = 0.44 \times 10^6$ $\alpha_m = 3.90^\circ$

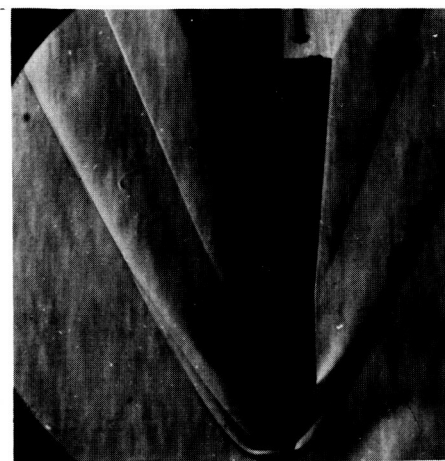


$R = 0.88 \times 10^6$ $\alpha_m = 3.25^\circ$

(b) Model 2.



$R = 0.44 \times 10^6$ $\alpha_m = 0^\circ$



$R = 0.88 \times 10^6$ $\alpha_m = 0^\circ$

Figure 5.- Continued.



$R = 0.44 \times 10^6$ $\alpha_m = 0^\circ$



$R = 0.44 \times 10^6$ $\alpha_m = 3.50^\circ$



$R = 0.44 \times 10^6$ $\alpha_m = 5.50^\circ$

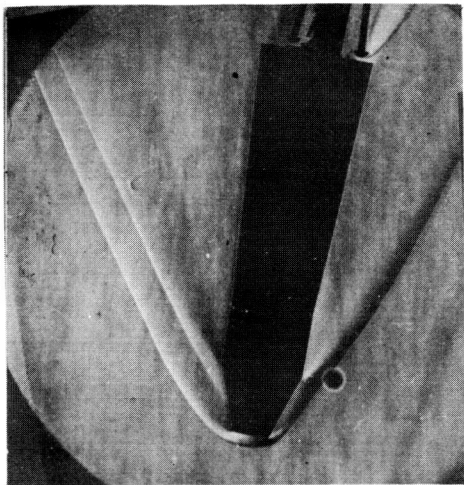


$R = 0.88 \times 10^6$ $\alpha_m = 3.20^\circ$

(c) Model 3.

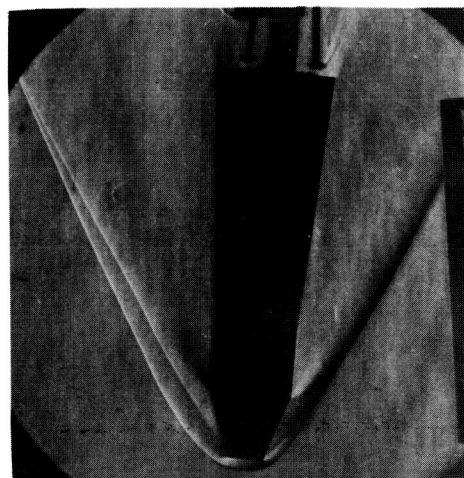
L-61-1075

03713 [REDACTED] 00



$OC_m = 7.55^\circ$

$R = 0.44 \times 10^6$



$OC_m = 4.00^\circ$

$R = 0.44 \times 10^6$



$OC_m = 0^\circ$

$R = 0.44 \times 10^6$



$OC_m = 3.35^\circ$

$R = 0.88 \times 10^6$



$OC_m = 0^\circ$

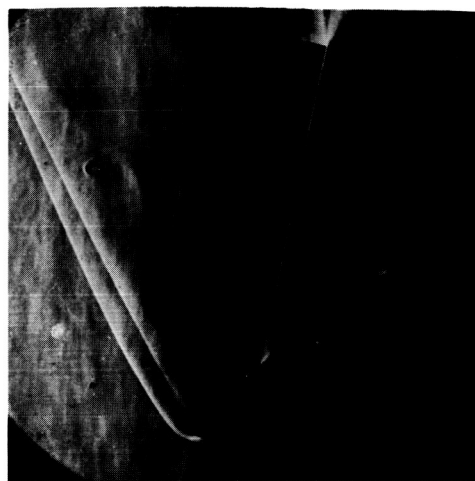
$R = 0.88 \times 10^6$

L-61-1076

(d) Model 4.

Figure 5.- Continued.

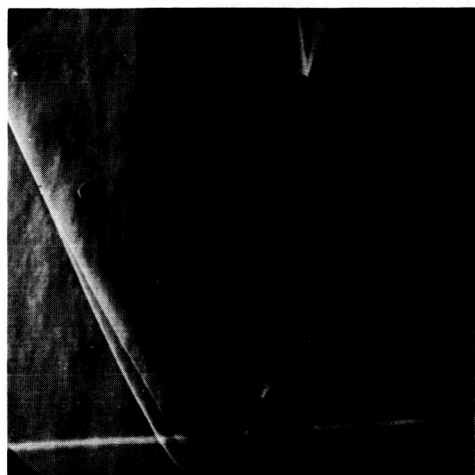
RECEIVED



$R = 0.44 \times 10^6$ $\alpha_m = 0^\circ$



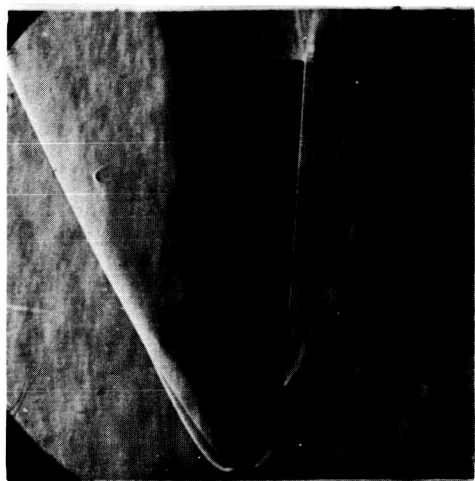
$R = 0.88 \times 10^6$ $\alpha_m = 8.35^\circ$



$R = 0.44 \times 10^6$ $\alpha_m = 4.45^\circ$



$R = 0.88 \times 10^6$ $\alpha_m = 5.00^\circ$



$R = 0.44 \times 10^6$ $\alpha_m = 10.95^\circ$

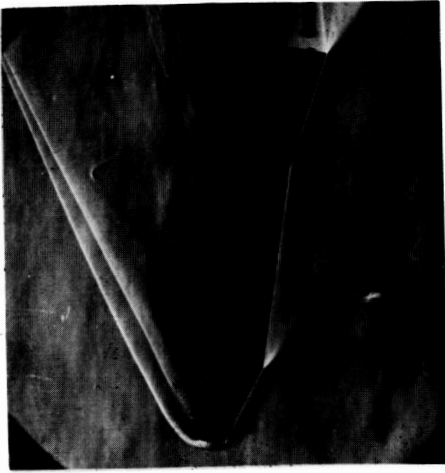


$R = 0.44 \times 10^6$ $\alpha_m = 10.95^\circ$

L-61-1077

(e) Model 5.

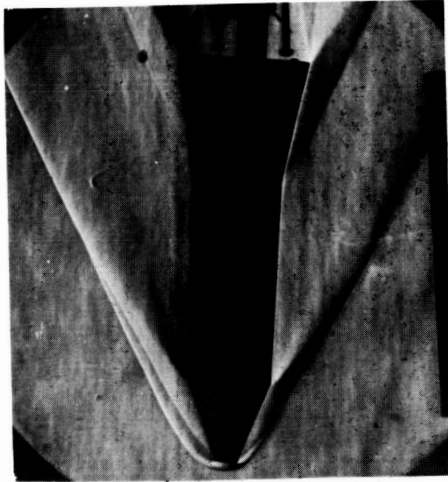
Figure 5.- Continued.



$R = 0.44 \times 10^6$ $\alpha_m = 7.60^\circ$



$R = 0.88 \times 10^6$ $\alpha_m = 5.90^\circ$



$R = 0.44 \times 10^6$ $\alpha_m = 3.80^\circ$



$R = 0.88 \times 10^6$ $\alpha_m = 3.50^\circ$



$R = 0.44 \times 10^6$ $\alpha_m = 0^\circ$



$R = 0.88 \times 10^6$ $\alpha_m = 0^\circ$

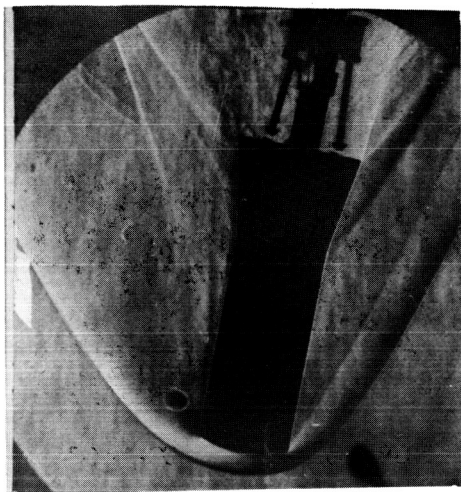
L-61-1078

(f) Model 6.

Figure 5.- Concluded.

RECEIVED

DECLASSIFIED



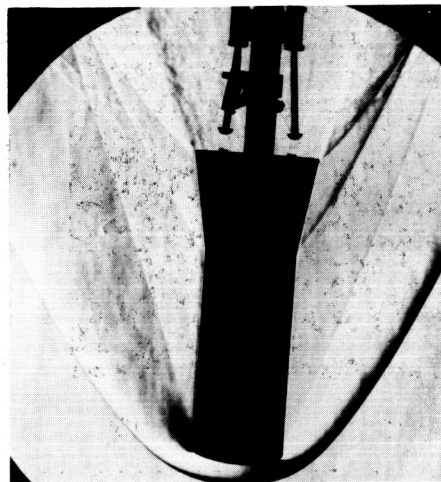
$\alpha_m = 11.00^\circ$

$R = 0.44 \times 10^6$



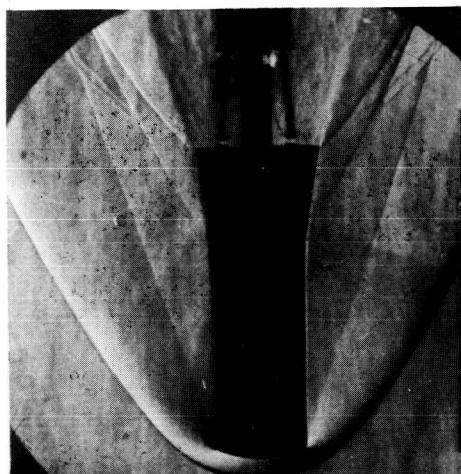
$\alpha_m = 8.75^\circ$

$R = 0.44 \times 10^6$



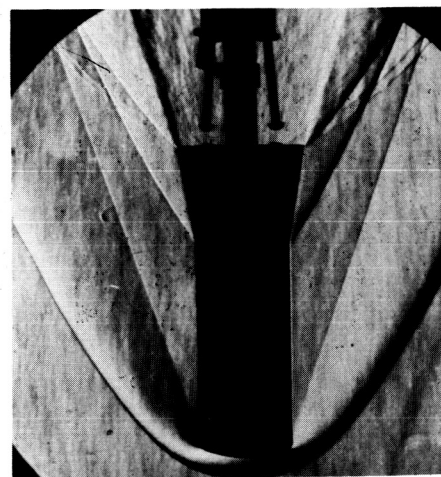
$\alpha_m = 4.05^\circ$

$R = 0.88 \times 10^6$



$\alpha_m = 0^\circ$

$R = 0.44 \times 10^6$



$\alpha_m = 0^\circ$

$R = 0.88 \times 10^6$

L-61-1079

Figure 6.- Typical schlieren photographs of model 7.

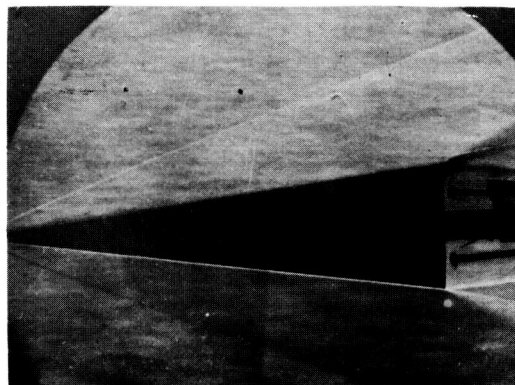
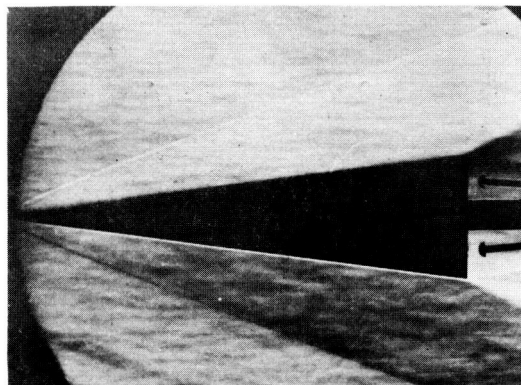
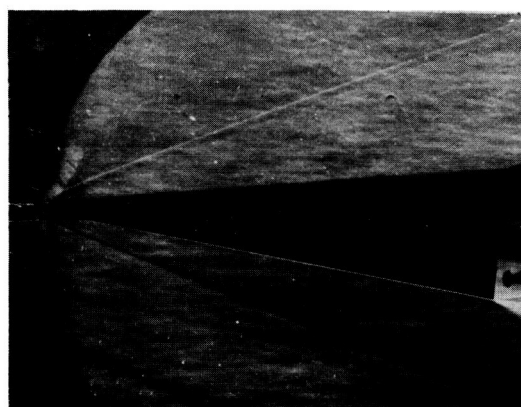
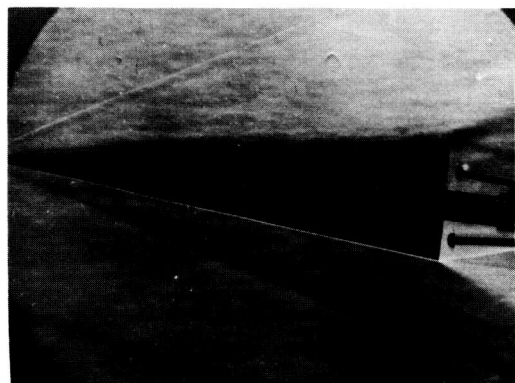
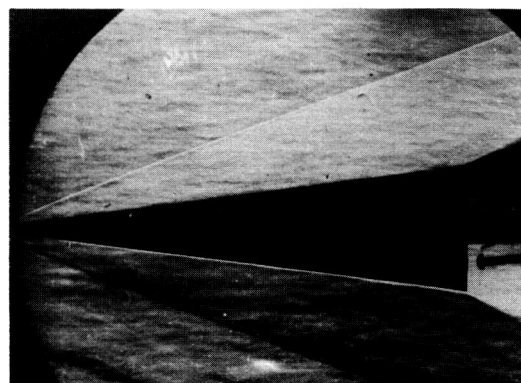
 $R = 0.44 \times 10^6$ $\alpha_m = 0^\circ$  $R = 0.88 \times 10^6$ $\alpha_m = 0^\circ$  $R = 0.44 \times 10^6$ $\alpha_m = 4.15^\circ$  $R = 0.88 \times 10^6$ $\alpha_m = 4.20^\circ$  $R = 0.44 \times 10^6$ $\alpha_m = 6.35^\circ$  $R = 1.32 \times 10^6$ $\alpha_m = 0^\circ$

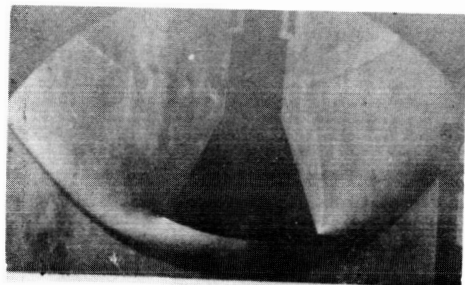
Figure 7.- Typical schlieren photographs of model 8. L-61-1080

RECLASSIFIED

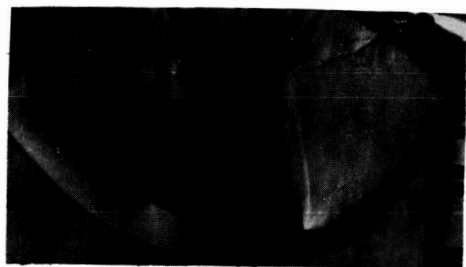
RECLASSIFIED



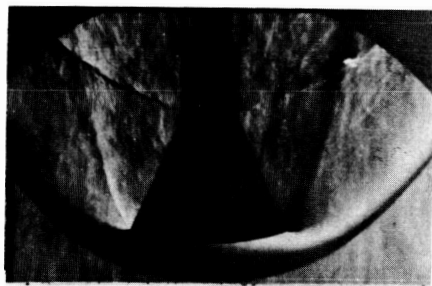
$R = 0.55 \times 10^6$ $\alpha_m = 0^\circ$



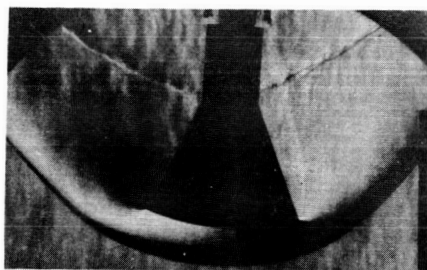
$R = 0.55 \times 10^6$ $\alpha_m = 4.75^\circ$



$R = 0.55 \times 10^6$ $\alpha_m = 8.60^\circ$



$R = 1.10 \times 10^6$ $\alpha_m = 0^\circ$

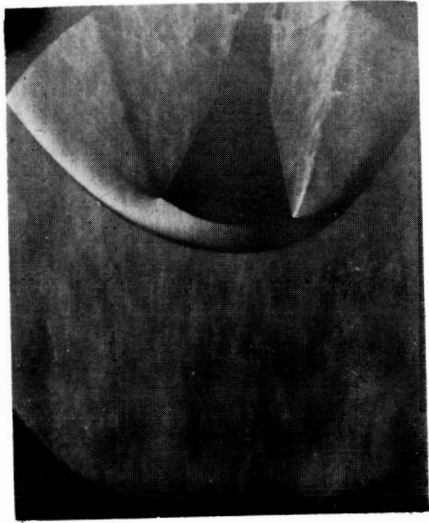
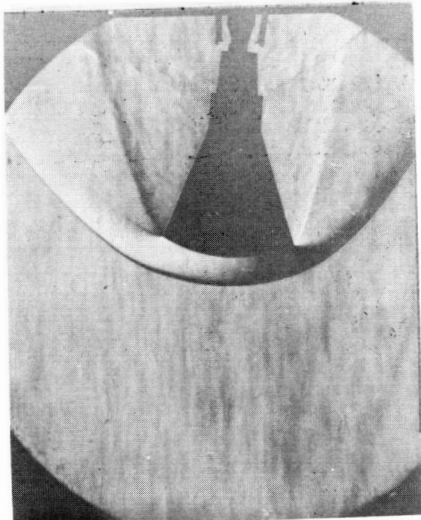
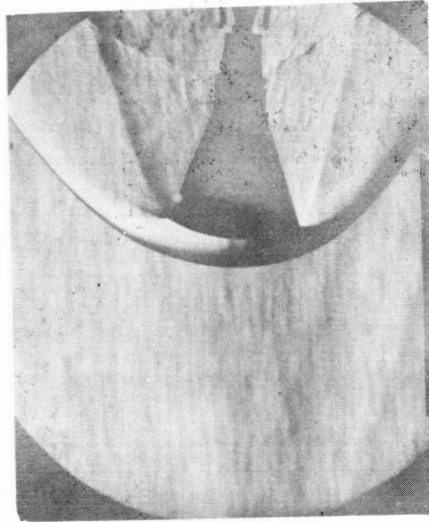
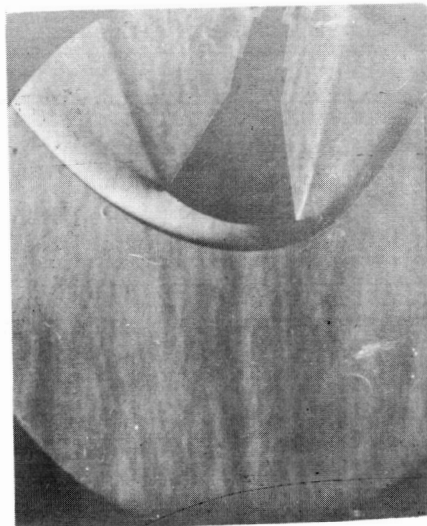


$R = 1.10 \times 10^6$ $\alpha_m = 3.65^\circ$

(a) Model 9.

L-61-1081

Figure 8.- Typical schlieren photographs of reentry capsule models.


 $R = 0.495 \times 10^6$
 $\alpha_m = 9.90^\circ$

 $R = 0.495 \times 10^6$
 $\alpha_c = 4.75^\circ$

 $R = 0.99 \times 10^6$
 $\alpha_m = 4.35^\circ$

 $R = 0.495 \times 10^6$
 $\alpha_m = 14.10^\circ$

(b) Model 11. L-61-1082

Figure 8.- Concluded.